Biosensors and Bioelectronics 25 (2010) 2194–2199

Contents lists available at ScienceDirect

Biosensors and Bioelectronics

journal homepage: www.elsevier.com/locate/bios

Functionalized single-walled carbon nanohorns for electrochemical biosensing

Xiaoqing Liu[a,b], Haijuan Li[a,b], Fuan Wang[a,b], Shuyun Zhu[a,b], Yuling Wang[a,b], Guobao Xu[a,*]

[a] State Key Laboratory of Electroanalytical Chemistry, Changchun Institute of Applied Chemistry, Chinese Academy of Sciences, 5625 Renmin Street, Changchun, Jilin 130022, PR China
[b] Graduate University of the Chinese Academy of Sciences, PR China

ARTICLE INFO

Article history:
Received 5 December 2009
Received in revised form 20 February 2010
Accepted 23 February 2010
Available online 3 March 2010

Keywords:
Carbon nanohorns
Carbon nanotubes
Noncovalent functionalization
Biosensors
Heme proteins

ABSTRACT

Single-walled carbon nanohorns (SWNHs), distinguished by their high purity and distinct structure, were noncovalently functionalized with poly(sodium 4-styrenesulfonate). The functionalized SWNHs were characterized by scanning electron microscopy, atomic force microscopy, ultraviolet–visible spectroscopy, Fourier transform infrared spectroscopy, Raman spectroscopy, and thermogravimetry. Heme protein myoglobin was adsorbed onto surface of functionalized SWNHs to prepare electrochemical biosensor. Surface assembly process and direct electrochemistry of immobilized myoglobin were investigated by electrochemical impedance spectroscopy and cyclic voltammetry, respectively. The proposed biosensor exhibited good electrocatalysis to the reduction of hydrogen peroxide. The response was linear over the range 3–350 μM with a detection limit of 0.5 μM. Good reproducibility and stability of the biosensor were obtained toward hydrogen peroxide detection.

© 2010 Elsevier B.V. All rights reserved.

1. Introduction

Nanostructured carbon materials such as carbon nanotubes (CNTs) have been extensively studied in electrochemistry and biosensors due to their excellent mechanical and electrical properties (Hu and Dong, 2008; Kato et al., 2008; Kim et al., 2007; McCreery, 2008; Tasis et al., 2006). CNTs can improve the electrochemical activity of biomolecules and redox proteins and have numerous applications (Chen et al., 2009; Katz and Willner, 2004; Merkoci et al., 2005; Wang and Lin, 2008). There are also different opinions concerning fundamental electroactive site of CNTs (Banks et al., 2005; Chou et al., 2005; Gong et al., 2008). However, CNTs often contain impurities, and the purification treatment will result in extra disadvantages for CNTs such as degradation, defects, loss of electronic and mechanical properties. Impurities such as metallic impurities in CNTs are difficult to remove even after extensive treatment (Pumera, 2007). In addition, metallic impurities will take part in the redox reaction of many biomarkers, resulting in potential experimental misinterpretations. It has been reported that metallic impurities within carbon nanotubes exhibit redox activity toward the oxidation of hydrazine (Banks et al., 2006; Pumera and Iwai, 2009a) and amino acids (Pumera et al., 2009). More seriously, these impurities can catalyze the electrochemical oxidation of glucose (Batchelor-McAuley et al., 2008; Siegert et al., 2009), which is a biologically vital molecules, and even can direct the reduction of hydrogen peroxide (Pumera and Iwai, 2009b; Sljukic et al., 2006), which is also one of the most important biomarkers and popular analytes for biosensing (Cass et al., 1984). As residual impurities may dominate electrochemical activity of CNTs in some cases, amount of metallic impurities in carbon nanotubes that can dominate redox properties is studied (Pumera and Miyahara, 2009). Noteworthily, high purity metal catalyst-free CNT (Jones et al., 2007) and multilayer graphene nanoflake films with sharp edge planes (Shang et al., 2008) have been smartly used to avoid the problem. The performance for dopamine detection at multilayer graphene nanoflake films with sharp edge planes is even comparable to that of edge plane pyrolytic graphite.

Single-walled carbon nanohorns (SWNHs) are horn-shaped sheath composed of single-wall graphene sheets. SWNHs have a conical structure with a particularly sharp apical angle. Different from CNTs, SWNHs usually assemble into roughly spherical aggregates with high surface area and excellent porosity (Iijima et al., 1999; Yang et al., 2005). The distinct structure of SWNHs conduces to novel mechanical and electronic properties, which have attracted considerable attention (Yudasaka et al., 2008). SWNHs are produced by the laser ablation of pure graphite with high yield in the absence of metal catalyst. The metal-free property of SWNHs is a significant advantage of SWNHs over CNTs in practical use, especially in electrochemistry to avoid potential interference from residual metal impurities. Because of their unique structures, high yield, high purity, and low toxicity (Isobe et al., 2006; Miyawaki et al., 2007), SWNHs have substantial promise for applications in many fields largely complementary to applications of carbon nanotubes. Furthermore, SWNHs have some prominent features

* Corresponding author. Tel.: +86 431 85262747; fax: +86 431 85262747.
E-mail address: guobaoxu@ciac.jl.cn (G. Xu).

0956-5663/$ – see front matter © 2010 Elsevier B.V. All rights reserved.
doi:10.1016/j.bios.2010.02.027

compared to CNTs (Yudasaka et al., 2008), therefore, SWNHs are attractive alternative to CNTs for biosensing (Kase et al., 2004; Zhu et al., 2003), electrochemical applications (Liu et al., 2008), and may suggest potential application in biofuel cell. However, the low solubility in conventional solvents hinders practical applications of SWNHs.

To overcome the problem of solubility and extend the application of SWNHs, covalent or noncovalent functionalization of SWNHs has been achieved. The covalent functionalization of SWNHs usually involves the decoration sidewalls of SWNHs with organic species such as pyrrolidine rings, porphyrin, and diblock copolymer by direct nucleophilic addition, amidation of the carboxyl groups, 1,3 dipolar cycloaddition, or anionic polymerization with the grafting-to approach (Cioffi et al., 2006, 2007; Mountrichas et al., 2007; Pagona et al., 2007a; Tagmatarchis et al., 2006). Another covalent method is based on opening of the cone-shaped tip of SWNHs and attachment of various organic amines, alcohols, and thiols to the cone-ends of SWNHs (Pagona et al., 2006a). The covalent functionalization can enhance solubilization and signify the potential application of SWNHs as electron acceptors for novel donor–acceptor nanosystems. However, the covalent functionalization will result in the perturbation of the continuous π-electronic network of SWNH. Noncovalent functionalization is another promising approach to improve the solubilization of SWNHs and explore application of SWNHs (Britz and Khlobystov, 2006; Chen et al., 2001). The supramolecular π–π stacking interactions between the sidewalls of SWNHs with pyrenes or porphyrins make SWNHs dispersed without significantly disrupting their π-electronic network (Zhu et al., 2003; Pagona et al., 2006b, 2007b,c). It is attractive to explore noncovalent method to extend the application of SWNHs. Polymers are appealing candidates for the formation of supramolecular complexes with carbon skeleton through noncovalent attachment (O'Connel et al., 2001; Zhao and Stoddart, 2009), because polymers usually have more involved interaction sites for surface adsorption (Jönsson-Niedziolka et al., 2009; Ugo et al., 2002).

In this study, we describe a new way for the noncovalent functionalization of SWNHs. A polymer named poly(sodium 4-styrenesulfonate) (PSS) was used to disperse SWNHs in aqueous solution. Myoglobin (Mb) is an oxygen-transport protein in mammalian muscle with a molecular weight of about 17,000 and a known structure (Rusling and Nassar, 1993; Li et al., 2006). It is generally much cheaper than peroxidases, and is very suitable for large scale production by recombinant means well known in the art. Extensive studies show that its activity can be greatly enhanced by suitable modification (Wan et al., 1998). The features above make Mb promising in hydrogen peroxide biosensors. Moreover, Mb has an isoelectric point (pI) of around 7.2, and can adsorb to negatively charged PSS easily (Ma et al., 2000). Therefore, the PSS modified SWNHs (PSS–SWNHs) were utilized to further assemble Mb to facilitate electrochemical communication between protein and composite modified electrode (Guiseppi-Elie et al., 2005; Rusling and Zhang, 2001). Application of the constructed biosensor for the determination of H_2O_2 was investigated. SWNHs exhibit favorable electrochemical properties in the experiment. The study will facilitate applications of SWNHs in the fields of biosensor and electrochemistry.

2. Experimental

2.1. Reagents

Dahlia-like SWNHs were prepared by CO_2 laser ablation. Mb from horse heart (90%, PhastGel) was purchased from Sigma and used as received. PSS (30 wt.%, Mw = 200,000 g/mol) was obtained from Aldrich. Other reagents were of analytical grade. All solutions were prepared with doubly deionized water.

2.2. Apparatus and measurements

Electrochemical measurements were carried out in a conventional three-electrode cell with an 832B potentiostat (CHI Inc., USA). The working electrode was a glassy carbon (GC) electrode. An Ag/AgCl electrode and a Pt wire were used as reference and counter electrode, respectively. During the course of the experiments, the solutions were first deoxygenated by bubbling ultra-pure nitrogen for 15 min, then were kept in a nitrogen atmosphere. Ultraviolet–visible (UV–vis) spectra were carried out using a Cary 500 UV-vis spectrometer (Varian Co., USA). Fourier transform infrared (FTIR) spectroscopy experiment was operated using BRUKER Vertex 70 FTIR (Germany). Raman spectra were recorded using a Renishaw system 2000 Raman spectrometer operating with an Ar^+ ion laser (514.5 nm). Transmission electron microscopy (TEM) measurements were performed using a JEOL 2010 transmission electron microscope operated at an accelerating voltage of 200 kV. Field-emission scanning electron microscopy (SEM) and energy-dispersive X-ray spectroscopy (EDS) measurements were carried out using a PHILIPS XL30 ESEM-FEG at an accelerating voltage of 20 kV. Tapping-mode atomic force microscopy (AFM) was conducted using an SPA400 equipped with an SPI3800N controller microscope instrument (made in Japan, Seiko Instruments, Inc.). Thermogravimetric analysis (TGA) was performed using a Pyris Diamond TG/DTA thermogravimetric analyzer (Perkin Elmer Thermal Analysis). Samples were heated under nitrogen atmosphere from 40 to 900 °C at 10 °C/min. Electrochemical impedance spectroscopy (EIS) was carried out using a Solartron 1255B Frequency Response Analyzer and a Solartron 1470 Battery Test Unit (Solartron Inc., UK), and 5 mM $K_3[Fe(CN)_6]/K_4[Fe(CN)_6]$ was used as a redox probe during the measurement. The direct current potential and alternating current amplitude were set at 0.22 and 5 mV, respectively.

2.3. Preparation of PSS–SWNHs

Polymer wrapping was performed by the reported method with variation (Correa-Duarte et al., 2004). SWNHs were dispersed in 1 wt.% aqueous solution of PSS to a concentration of 0.05 mg ml^{-1} by strong sonication. The dispersed solution was stored at 50 °C for 12 h. Excess PSS was removed through repeated centrifugation and redispersion cycles, and stable colloid of PSS–SWNHs in water was obtained.

2.4. Preparation of Mb/PSS–SWNH/GC and Mb/SWNH/GC electrodes

Before modification, the bare GC electrode was polished with 0.05-μm alumina slurry, sonicated in deionized water, and then dried in highly purified nitrogen stream. PSS–SWNH/GC electrode was made by dropping 0.2 mg ml^{-1} of PSS–SWNHs onto bare GC electrode, dried at room temperature, and thoroughly rinsed with water. Mb/PSS–SWNH/GC electrode was fabricated by immersing the PSS–SWNH/GC electrodes in 1 mg ml^{-1} of Mb solution (pH 5.5) for about 3 h. Mb/SWNH/GC electrode was prepared in a similar way, and the difference is that pristine SWNH dissolved in dimethylformamide instead of PSS–SWNH dissolved in water is used. The modified electrode was rinsed with buffer and stored at 4 °C.

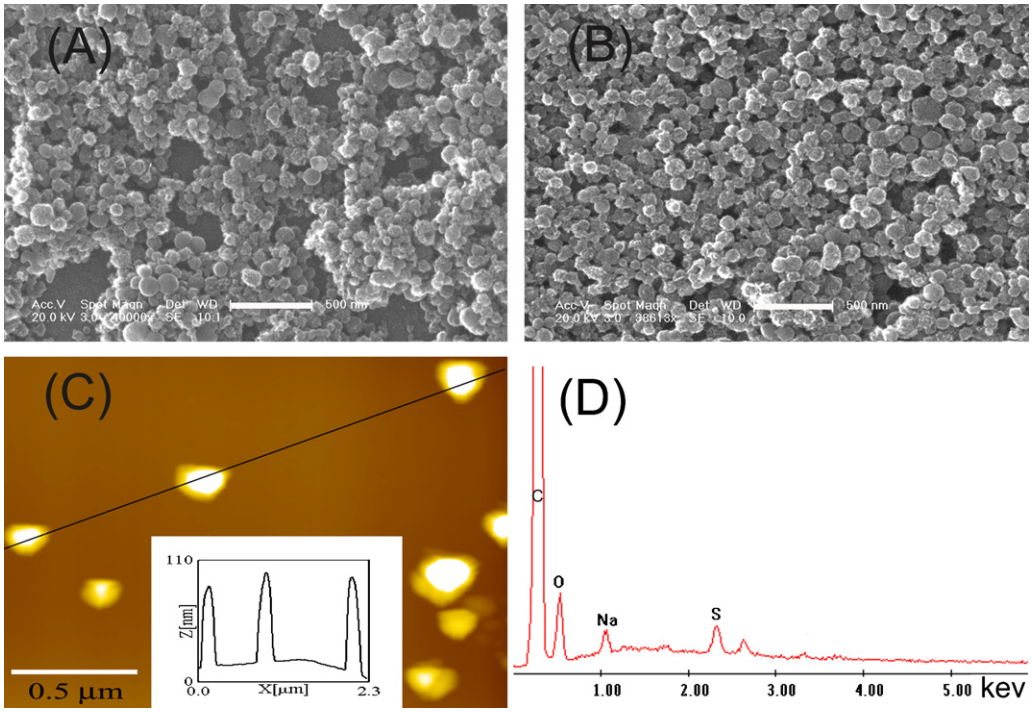

Fig. 1. (A and B) SEM images of SWNHs (A) and PSS–SWNHs (B) on GC electrode. (C) AFM image of PSS–SWNHs on mica. Insert: cross-sectional profile of the AFM image along the black line. (D) EDS pattern of PSS–SWNHs. The scale bar is 500 nm.

3. Results and discussion

3.1. Morphology and spectroscopy characterization of PSS–SWNHs

SWNHs generally exist as spherical aggregates (Fig. S1) and the SWNH aggregates have low solubility in water. After functionalization, solubility of SWNHs increased and the homogeneous black solution of PSS–SWNHs was stable for over a month. The improved solubility is based on the thermodynamic preference of PSS–SWNH interaction (Correa-Duarte et al., 2004; O'Connel et al., 2001). Hydrophobic portion of PSS can cover surface of SWNHs to eliminate hydrophobic interface between SWNHs and their aqueous medium (Correa-Duarte and Liz-Marzan, 2006). Scanning electron microscopy, atomic force microscopy, ultraviolet–visible spectroscopy, Fourier transform infrared spectroscopy, Raman spectroscopy, and thermogravimetry were used to characterize PSS–SWNHs in the following experiments. Fig. 1(A and B) shows that both pristine SWNHs and PSS–SWNHs assemble into spherical nanostructures, suggesting that the noncovalent functionalization does not significantly alter the morphology of SWNHs. The PSS–SWNH composite has also been investigated by AFM (Fig. 1C). Representative image showed that individual spherical aggregate of PSS–SWNHs was 70–85 nm in height. The result demonstrates that the average diameter of spherical aggregate is consistent with the particle size obtained by SEM. The presence of PSS is confirmed by EDS (Fig. 1D). The major element of O, S and Na indicated that PSS was functionalized onto the surface of SWNHs.

Fig. 2 displays UV–vis spectra of SWNHs, PSS–SWNHs and PSS. The absorption band for SWNHs appeared at 262 nm with a broad peak, and the spectrum of PSS displayed a strong absorbance at 225 nm and a minor absorption band at 261 nm. The UV–vis spectrum of PSS–SWNHs exhibited a sharp absorption peak at 225 nm, implying the wrapping of PSS onto SWNHs (Zhou et al., 2004). Fig. S2A compares FTIR spectrum of SWNHs and PSS–SWNHs. The spectrum of PSS–SWNHs is in agreement with typical spectrum of PSS. The characteristic peaks of the bands for PSS–SWNHs at 1171 and 1375 cm^{-1} were ascribed to sulfonic group. Peaks at around 1462, 1536, and 1575 cm^{-1} were ascribed to benzene group. The C–H stretching and bending active vibrations were identified at about 2844, 2915, 2950 and 3064 cm^{-1}. The spectral analysis suggests that PSS can either thread themselves onto or wrap themselves around the surface of SWNHs, similar to the interactions between polymers and CNTs.

Raman spectroscopy of PSS–SWNHs reveals the presence of two prominent bands at 1334 cm^{-1} (D-band) and 1580 cm^{-1} (G-band), which is characteristic of SWNHs (Fig. S2B). The G-band is related to the vibrations of the sp^2-hybridized carbon network. The D-band is attributed to the loss of basal plane lattice periodicity of SWNHs and to the sp^3 single-bonding carbon atoms existing within aggregates (Cioffi et al., 2007). Relative intensity of the D-band to the G-band can monitor the density of defects generated on the network of SWNHs after functionalization. The spectroscopy revealed that the

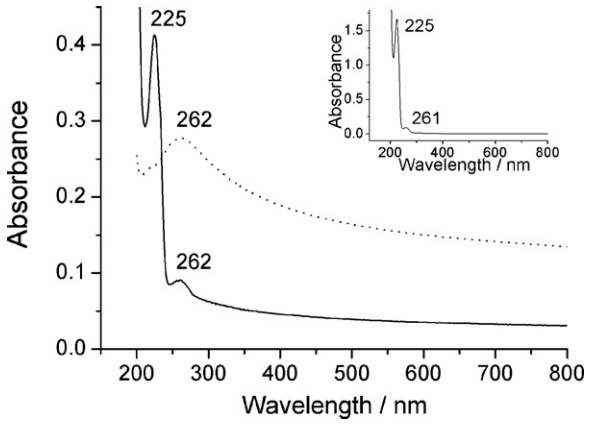

Fig. 2. UV–vis absorption spectra of SWNHs (dotted line) and PSS–SWNHs (solid line) monitored in aqueous solutions. Insert: absorbance of PSS in aqueous solution.

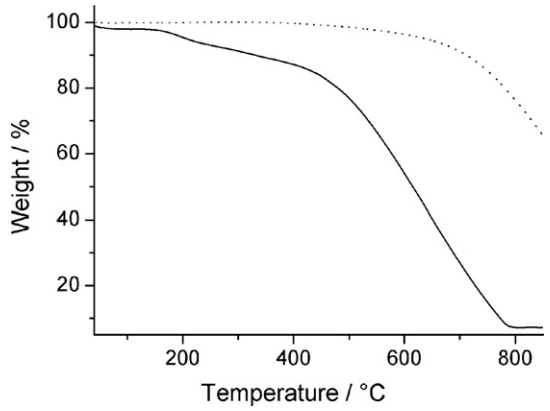

Fig. 3. TGA of SWNHs (dotted line) and PSS–SWNHs (solid line).

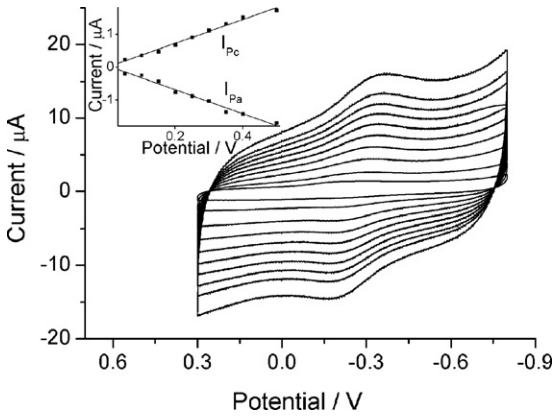

Fig. 5. Cyclic voltammograms of Mb/PSS–SWNH/GC electrode in 0.1 M (pH 5.5) acetate buffer solution at different scan rates. Insert: dependence of anodic and cathodic peak currents on scan rate.

relative intensity for the two peaks showed little change after functionalization. The comparison indicated the noncovalent nature of interactions between SWNHs and PSS (Pagona et al., 2007b).

The amount of PSS in the functionalized SWNHs was evaluated by TGA (Fig. 3). Pristine SWNHs had good thermal stability below 645 °C under nitrogen. A loss of weight corresponding to PSS wrapped on SWNHs was about 69% at 800 °C. Such a loss demonstrated that the functionalization percentage of the SWNHs with polymer was about 0.013% (molar percentage, molecular weight of PSS: 200,000 g/mol). The result is consistent with the unchanged relative intensity for D-band and G-band in Raman spectroscopy.

3.2. Assembly process and electrochemical properties of Mb immobilized on PSS–SWNHs

The use of functionalized SWNHs in electrochemical biosensor was investigated. Heme protein Mb was assembled onto PSS–SWNHs modified electrode and electrochemistry of immobilized Mb was studied. The surface assembly process of Mb was monitored by EIS. When PSS–SWNHs were modified on electrode, the charge-transfer resistance (Rct, the diameter of the semicircle in the Nyquist plot) was greatly decreased compared with that on bare electrode, indicating that the film had good conductivity (Fig. 4, curves a and b). After adsorption of Mb onto the PSS–SWNHs, a significant increase in Rct was observed. Moreover, the longer the adsorption time, the larger the Rct (Fig. 4, curves c, d, and e). The significant impedance changes imply that Mb has been assembled on the electrode surface. Other interactions such as

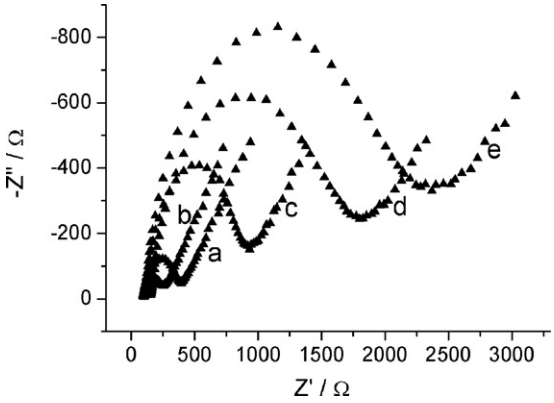

Fig. 4. Nyquist plots of bare GC electrode (a), PSS–SWNH/GC electrode (b), and Mb/PSS–SWNH/GC electrode fabricated by immersing PSS–SWNH/GC electrode in Mb solution for 2 h (c), 3 h (d), and 4 h (e).

π–π stacking interactions and hydrophobic interactions may also exist between Mb and PSS–SWNHs (Azamian et al., 2002; Lin et al., 2004).

Cyclic voltammograms shows that a pair of well-defined redox peaks appears when Mb is adsorbed on PSS–SWNH modified electrode, whereas no peak is observed at PSS–SWNH modified electrode (Fig. S3). The comparison implies a favorable orientation of Mb at PSS–SWNH modified electrode. By integration of the reduction peaks according to the following equation:

$$Q = nFA\Gamma$$

where Q is the charge involved in the reaction, n is the number of electron transferred, F is the Faraday's constant, and A is the surface area of the GC electrode, the active Mb adsorbed on the electrode surface is calculated to be 9.94×10^{-11} mol cm^{-2} (geometric area is employed). The value of the surface coverage was larger than the theoretical monolayer coverage of 1.58×10^{-11} mol cm^{-2} for Mb estimated from the crystallographic data (Kendrew et al., 1958), comparable with 5.18×10^{-11} mol cm^{-2} for heme proteins entrapped in agarose hydrogel films (Liu et al., 2004a) and 8.85×10^{-11} mol cm^{-2} for a core–shell nanocluster films containing polyelectrolyte and silica nanoparticles (Liu et al., 2004b). The larger surface coverage may be due to three-dimensional nanostructured morphology of SWNHs.

The direct electrochemistry of Mb is demonstrated through cyclic voltammetry by varying scan rate and solution pH. Fig. 5 shows that the formal potential is -0.270 ± 0.005 V under different scan rates, which agrees well with those obtained from Mb entrapped in polyacrylamide hydrogel films (Shen et al., 2002), Mb–titanate nanotubes composite film, and Mb–titanium oxide anatase nanoparticles film cast on basal plane pyrolytic graphite electrode (Liu et al., 2005). When scan rates were increased from 0.02 to 0.5 V s^{-1}, both the anodic and the cathodic peak currents were proportional to scan rate, suggesting a typical surface controlled electrode process for the electron transfer of Mb on the electrode. When scan rate was larger than 0.5 V s^{-1}, the peak-to-peak separation (ΔEp) became larger than 0.2 V, and ΔEp increased rapidly with increased scan rate (Fig. S4). When $n\Delta E\text{p} \geq 0.2$ V, the direct electron transfer rate constants (ks) can be estimated from the Laviron model equation (Laviron, 1979):

$$\Delta E_{\text{P}} = \frac{RT}{nF\alpha(1-\alpha)} \ln \nu + \frac{RT}{nF\alpha(1-\alpha)} \ln(1-\alpha) + \frac{RT}{nF\alpha} \ln \alpha - \frac{1}{\alpha(1-\alpha)} \ln \left(\frac{RT}{nF}\right)^{(RT/nF)} - \frac{RT}{nF\alpha(1-\alpha)} \ln k_S$$

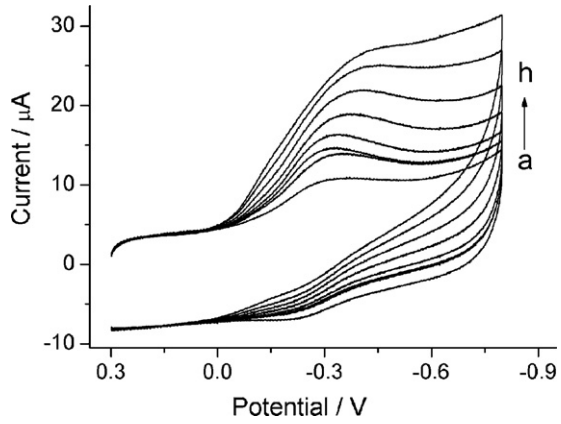

Fig. 6. Cyclic voltammograms of the Mb/PSS–SWNH/GC electrode in the presence of 0 μM (a), 3 μM (b), 5 μM (c), 10 μM (d), 100 μM (e), 150 μM (f), 300 μM (g), and 350 μM (h) H_2O_2 in 0.1 M (pH 5.5) acetate buffer solution. Scan rate: 0.2 V s^{-1}.

Here α is charge-transfer coefficient and n is the number of electrons transferred in the reaction. The electron transfer rate constant was calculated about 3.50 s^{-1}, which was larger than the value for Mb immobilized in biocompatible silk fibroin film (1.34 s^{-1}) (Wu et al., 2006). This indicates a fast electron transfer between the immobilized electroactive centers of Mb and PSS–SWNH modified electrode. It can be attributed to the fact that the nanostructured spherical PSS–SWNHs provide a favorable microenvironment for Mb and the good conductivity of SWNHs facilitates electron tunneling. Further study showed that cyclic voltammograms of Mb/PSS–SWNH/GC electrode depended on solution pH. The formal potential decreased linearly as pH increased from 4.0 to 8.0. Slope of the line was −0.43 V pH^{-1} and the value was close to theoretical value for the reversible one electron-transfer coupled by single-proton transportation (Bond, 1980). The electron process can be can be expressed by the following equation:

$$\text{MbhemeFe(III)} + H^+ \rightarrow \text{MbhemeFe(II)}$$

Fig. 6 and Figs. S5 and S6 show the cyclic voltammograms at the Mb/PSS–SWNH/GC electrode and the Mb/SWNH/GC electrode as well as the corresponding calibration curves, respectively. By comparison, the Mb/PSS–SWNH/GC sensor is much more sensitive than the Mb/SWNH/GC sensor. The best linear relationship was obtained from 3 to 350 μM H_2O_2 with a detection limit of 0.5 μM H_2O_2 for the Mb/PSS–SWNH/GC sensor. The sensitivity of H_2O_2 is much lower than that at the soybean peroxidase/SWNH biosensor (Shi et al., 2009) and that at activated SWNH paste electrode (Zhu et al., 2008). The relative standard deviation value of the measured cathodic current for 10 successive assays of 10 μM H_2O_2 was 3.5%. The biosensor displays almost unchanged current response to H_2O_2 when stored at 4 °C over a week, and retains 80% of the initial response toward H_2O_2 after storing for half a month. The good reproducibility and stability of the biosensor indicate that PSS–SWNHs can efficiently retain electrocatalytic activity of Mb. The electrocatalytic current began to level off with further increase of H_2O_2 concentration. The apparent Michaelis–Menten constant K_m^{app} was 400.5 μM obtained from Lineweaver–Burk equation (Kamin and Wilson, 1980).

$$I^{-1} = K_m^{app}\ I_{max}^{-1}\ c^{-1} + I_{max}^{-1}$$

where I, I_{max}, and c stand for the steady-state current after addition of substrate, the maximum current measured under saturated substrate, and the bulk concentration of substrate, respectively. The results are comparable with Mb entrapped in titanate nanotubes film (Liu et al., 2005) and Mb bound to interlayer of magadiite (Peng et al., 2004).

4. Conclusion

This work describes functionalization of SWNHs with polymer PSS through noncovalent interaction. The functionalization improves solubility of SWNHs and facilitates electrochemical application of SWNHs. The electron transfer of Mb immobilized on PSS–SWNH modified electrode was a surface controlled process involving in a reversible, one electron coupled one-proton reaction process. The constructed biosensor exhibited good electrocatalytic response, nice reproducibility, and good stability for the determination of H_2O_2. The study shows that SWNH is a good candidate for constructing sensor and biosensor.

Acknowledgements

We thank the group of Prof. S. Iijima (Solution Oriented Research for Science and Technology in Japan Science and Technology Agency) for generous offer of SWNHs. The work was supported by the National Natural Science Foundation of China (Nos. 20875086 and 20505016), the Department of Sciences and Technology of Jilin Province (Nos. 20070108 and 20082104) and the Ministry of Science and Technology of the People's Republic of China (No. 2006BAE03B08).

Appendix A. Supplementary data

Supplementary data associated with this article can be found, in the online version, at doi:10.1016/j.bios.2010.02.027.

References

Azamian, B.R., Davis, J.J., Coleman, K.S., Bagshaw, C.B., Green, M.L.H., 2002. J. Am. Chem. Soc. 124, 12664–12665.
Banks, C.E., Crossley, A., Salter, C., Wilkins, S.J., Compton, R.G., 2006. Angew. Chem. Int. Ed. 45, 2533–2537.
Banks, C.E., Davies, T.J., Wildgoose, G.G., Compton, R.G., 2005. Chem. Commun. 7, 829–841.
Batchelor-McAuley, C., Wildgoose, G.G., Compton, R.G., Shao, L., Green, M.L.H., 2008. Sens. Actuators B 132, 356–360.
Bond, A.M., 1980. Modern Polarographic Methods in Analytical Chemistry. Marcel Dekker, New York, pp. 29–30.
Britz, D.A., Khlobystov, A.N., 2006. Chem. Soc. Rev. 35, 637–659.
Cass, A.E.G., Davis, G., Francis, G.D., Hill, H.A.O., Aston, W.J., Higgins, I.J., Plotkin, E.V., Scott, L.D.L., Turner, A.P.F., 1984. Anal. Chem. 56, 667–671.
Chen, H., Jiang, C., Yu, C., Zhang, S., Liu, B., Kong, J., 2009. Biosens. Bioelectron. 24, 3399–3411.
Chen, R.J., Zhan, Y.G., Wang, D.W., Dai, H.J., 2001. J. Am. Chem. Soc. 123, 3838–3839.
Chou, A., Bocking, T., Singh, N.K., Gooding, J.J., 2005. Chem. Commun. 7, 842–844.
Cioffi, C., Campidelli, S., Brunetti, F.G., Meneghetti, M., Prato, M., 2006. Chem. Commun. 20, 2129–2131.
Cioffi, C., Campidelli, S., Sooambar, C., Marcaccio, M., Marcolongo, G., Meneghetti, M., Paolucci, D., Paolucci, F., Ehli, C., Rahman, G.M.A., Sgobba, V., Guldi, D.M., Prato, M., 2007. J. Am. Chem. Soc. 129, 3938–3945.
Correa-Duarte, M.A., Liz-Marzan, L.M., 2006. J. Mater. Chem. 16, 22–25.
Correa-Duarte, M.A., Sobal, N., Liz-Marzan, L.M., Giersig, M., 2004. Adv. Mater. 16, 2179–2184.
Gong, K., Chakrabarti, S., Dai, L., 2008. Angew. Chem. Int. Ed. 47, 5446–5450.
Guiseppi-Elie, A., Brahim, S., Wnek, G., Baughman, R., 2005. Nanobiotechnology 1, 83–92.
Hu, X., Dong, S., 2008. J. Mater. Chem. 18, 1279–1295.
Iijima, S., Yudasaka, M., Yamada, R., Bandow, S., Suenaga, K., Kokai, F., Takahashi, K., 1999. Chem. Phys. Lett. 309, 165–170.
Isobe, H., Tanaka, T., Maeda, R., Noiri, E., Solin, N., Yudasaka, M., Iijima, S., Nakamura, E., 2006. Angew. Chem. Int. Ed. 45, 6676–6680.
Jones, C.P., Jurkschat, K., Crossley, A., Compton, R.G., Riehl, B.L., Banks, C.E., 2007. Langmuir 23, 9501–9504.
Jönsson-Niedziolka, M., Szot, K., Rogalski, J., Opallo, M., 2009. Electrochem. Commun. 11, 1042–1044.
Kamin, R.A., Wilson, G.S., 1980. Anal. Chem. 52, 1198–1205.
Kase, D., Kulp III, J.L., Yudasaka, M., Evans, J.S., Iijima, S., Shiba, K., 2004. Langmuir 20, 8939–8941.
Kato, D., Sekioka, N., Ueda, A., Kurita, R., Hirono, S., Suzuki, K., Niwa, O., 2008. J. Am. Chem. Soc. 130, 3716–3717.
Katz, E., Willner, I., 2004. ChemPhysChem 5, 1084–1104.
Kendrew, J.C., Bodo, G., Dintzis, H.M., Parrish, R.G., Wyckoff, H., Phillips, D.C., 1958. Nature 181, 662–666.

Kim, S.N., Rusling, J.F., Papadimitrakopoulos, F., 2007. Adv. Mater. 19, 3214–3228.
Laviron, E., 1979. J. Electroanal. Chem. 101, 19–28.
Li, N., Xu, J.-Z., Yao, H., Zhu, J.-J., Chen, H.-Y., 2006. J. Phys. Chem. B 110, 11561–11565.
Lin, Y., Taylor, S., Li, H., Fernando, K.A.S., Qu, L., Wang, W., Gu, L., Zhou, B., Sun, Y.P., 2004. J. Mater. Chem. 14, 527–541.
Liu, A., Wei, M., Honma, I., Zhou, H., 2005. Anal. Chem. 77, 8068–8074.
Liu, H.H., Tian, Z.Q., Lu, Z.X., Zhang, Z.L., Zhang, M., Pang, D.W., 2004a. Biosens. Bioelectron. 20, 294–304.
Liu, H.Y., Rusling, J.F., Hu, N.F., 2004b. Langmuir 20, 10700–10705.
Liu, X., Shi, L., Niu, W., Li, H., Xu, G., 2008. Biosens. Bioelectron. 23, 1887–1890.
Ma, H.Y., Hu, N.F., Rusling, J.F., 2000. Langmuir 16, 4969–4975.
McCreery, R.L., 2008. Chem. Rev. 108, 2646–2687.
Merkoci, A., Pumera, M., Llopis, X., Perez, B., del Valle, M., Alegret, S., 2005. Trends Anal. Chem. 24, 826–838.
Miyawaki, J., Yudasaka, M., Azami, T., Kubo, Y., Iijima, S., 2007. ACS Nano 2, 213–226.
Mountrichas, G., Pispas, S., Tagmatarchis, N., 2007. Chem. Eur. J. 13, 7595–7599.
O'Connel, M.J., Boul, P., Ericson, L.M., Huffman, C., Wang, Y., Haroz, E., Kuper, C., Tour, J., Ausman, K.D., Smalley, R.E., 2001. Chem. Phys. Lett. 342, 265–271.
Pagona, G., Fan, J., Maigne, A., Yudasaka, M., Iijima, S., Tagmatarchis, N., 2007b. Diamond Relat. Mater. 16, 1150–1153.
Pagona, G., Sandanayaka, A.S.D., Araki, Y., Fan, J., Tagmatarchis, N., Charalambidis, G., Coutsolelos, A.G., Boitrel, B., Yudasaka, M., Iijima, S., Ito, O., 2007a. Adv. Funct. Mater. 17, 1705–1711.
Pagona, G., Sandanayaka, A.S.D., Araki, Y., Fan, J., Tagmatarchis, N., Yudasaka, M., Iijima, S., Ito, O., 2006b. J. Phys. Chem. B 110, 20729–20732.
Pagona, G., Sandanayaka, A.S.D., Maigne, A., Fan, J., Papavassiliou, G.C., Petsalakis, I.D., Steele, B.R., Yudasaka, M., Iijima, S., Tagmatarchis, N., Ito, O., 2007c. Chem. Eur. J. 13, 7600–7607.
Pagona, G., Tagmatarchis, N., Fan, J., Yudasaka, M., Iijima, S., 2006a. Chem. Mater. 18, 3918–3920.
Peng, S., Gao, Q., Wang, Q., Shi, J., 2004. Chem. Mater. 16, 2675–2684.
Pumera, M., 2007. Langmuir 23, 6453–6458.
Pumera, M., Iwai, H., 2009a. J. Phys. Chem. C 113, 4401–4405.
Pumera, M., Iwai, H., 2009b. Chem. Asian J. 4, 554–560.
Pumera, M., Iwai, H., Miyahara, Y., 2009. ChemPhysChem 10, 1770–1773.
Pumera, M., Miyahara, Y., 2009. Nanoscale 1, 260–265.
Rusling, J.F., Nassar, A.-E.F., 1993. J. Am. Chem. Soc. 115, 11891–11897.
Rusling, J.F., Zhang, Z., 2001. In: Nalwa, R.W. (Ed.), Handbook of Surfaces and Interfaces of Materials, vol. 5: Biomolecules, Biointerfaces, and Application. Academic Press, San Diego, pp. 33–71.
Shang, N.G., Papakonstantinou, P., McMullan, M., Chu, M., Stamboulis, A., 2008. Adv. Funct. Mater. 18, 3506–3514.
Shen, L., Huang, R., Hu, N.F., 2002. Talanta 56, 1131–1139.
Shi, L., Liu, X., Niu, W., Li, H., Han, S., Chen, J., Xu, G., 2009. Biosens. Bioelectron. 24, 1159–1163.
Siegert, L., Kampouris, D.K., Kruusma, J., Sammelselg, V., Banks, C.E., 2009. Electroanalysis 21, 48–51.
Sljukic, B., Banks, C.E., Compton, R.G., 2006. Nano Lett. 6, 1556–1558.
Tagmatarchis, N., Maigne, A., Yudasaka, M., Iijima, S., 2006. Small 2, 490–494.
Tasis, D., Tagmatarchis, N., Bianco, A., Prato, M., 2006. Chem. Rev. 106, 1105–1136.
Ugo, P., Zangrando, V., Moretto, L.M., Brunetti, B., 2002. Biosens. Bioelectron. 17, 479–487.
Wan, L.L., Twitchett, M.B., Eltis, L.D., Mauk, A.G., Smith, M., 1998. Proc. Natl. Acad. Sci. U.S.A. 95, 12825–12831.
Wang, J., Lin, Y., 2008. Trends Anal. Chem. 27, 619–626.
Wu, Y.H., Shen, Q.C., Hu, S.S., 2006. Anal. Chim. Acta 558, 179–186.
Yang, C.M., Noguchi, H., Murata, K., Yudasaka, M., Hashimoto, A., Iijima, S., Kaneko, K., 2005. Adv. Mater. 17, 866–870.
Yudasaka, M., Iijima, S., Crespi, V.H., 2008. Top. Appl. Phys. 111, 605–629.
Zhao, Y.-L., Stoddart, J.F., 2009. Acc. Chem. Res. 42, 1161–1171.
Zhou, D., Bruckbauer, A., Batchelor, M., Kang, D.J., Abell, C., Klenerman, D., 2004. Langmuir 20, 9089–9094.
Zhu, J., Kase, D., Shiba, K., Kasuya, D., Yudasaka, M., Iijima, S., 2003. Nano Lett. 3, 1033–1036.
Zhu, S., Fan, L., Liu, X., Shi, L., Li, H., Han, S., Xu, G., 2008. Electrochem. Commun. 10, 695–698.